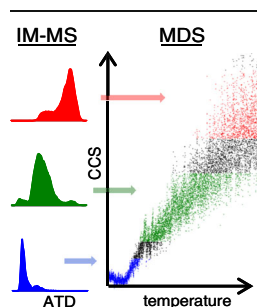RESEARCH ARTICLE

How Closely Related Are Conformations of Protein Ions Sampled by IM-MS to Native Solution Structures?

Shu-Hua Chen, David H. Russell

Department of Chemistry, Texas A&M University, College Station, TX 77843, USA

Abstract. Here, we critically evaluate the effects of changes in the ion internal energy (E_{int}) on ion-neutral collision cross sections (CCS) of ions of two structurally diverse proteins, specifically the $[M + 6H]^{6+}$ ion of ubiquitin (ubq^{6+}), the $[M + 5H]^{5+}$ ion of the intrinsically disordered protein (IDP) apo-metallothionein-2A (MT), and its partially- and fully-metalated isoform, the $[Cd_iMT]^{5+}$ ion. The ion-neutral CCS for ions formed by "native-state" ESI show a strong dependence on E_{int}. Collisional activation is used to increase E_{int} prior to the ions entering and within the traveling wave (TW) ion mobility analyzer. Comparisons of experimental CCSs with those generated by molecular dynamics (MD) simulation for solution-phase ions and solvent-free ions as a function of temperature provide new insights about conformational preferences and retention of solution conformations. The E_{int}-dependent CCSs, which reveal increased conformational diversity of the ion population, are discussed in terms of folding/unfolding of solvent-free ions. For example, ubiquitin ions that have low internal energies retain native-like conformations, whereas ions that are heated by collisional activation possess higher internal energies and yield a broader range of CCS owing to increased conformational diversity due to losses of secondary and tertiary structures. In contrast, the CCS profile for the IDP apoMT is consistent with kinetic trapping of an ion population composed of a wide range of conformers, and as the E_{int} is increased, these structurally labile conformers unfold to an elongated conformation.

Keywords: Ion mobility collision cross section, Ion internal energy, Native mass spectrometry

Introduction

The function and activity of cellular proteins is determined by their three-dimensional (3-D) structure, but correlating function and structure is immensely challenging owing to the fact that the native-state(s) of many proteins related to human diseases are disordered [1–3]. A high percentage (~40%) of all human proteins are partially or completely disordered [4], and many intrinsically disordered proteins (IDP) play important roles in disease mechanisms [5, 6], including p53 regulation in cancer pathways, amyloid beta (Aβ) and tau protein aggregation in Alzheimer's disease, α-synuclein in Parkinson's disease, and ~80% of cancer-associated and ~65% of cell-signaling proteins [7]. It is thought that structural flexibility and plasticity (disorder) provide

functional advantage [2, 3], which enhances a wide range of physiological pathways involving a disorder-to-order structural transition [8]. Characterization of IDP is challenging because they are inherently difficult to crystallize [9], and conformational diversity (disorder) complicates NMR approaches [10]. Consequently, there is increasing interest in developing mass spectrometry-based approaches for characterizing IDPs. Proteomic mass spectrometry (MS) approaches combined with hydrogen-deuterium exchange (HDX) [11–13] and chemical derivatization [14–16] provide high throughput, high sensitivity, and versatile strategies for protein structure characterization [17, 18]. These approaches are complemented by combining "native-ESI" and ion mobility-mass spectrometry (IM-MS) by providing ion collision cross section (CCS), a direct measure of the physical size and shape of the ions, for studies of conformational heterogeneity [19], elucidation of protein and protein complex conformations [20, 21], and characterization of IDPs [22–29]. Although there is mounting evidence that gas-phase ions formed by ESI retain elements of solution-phase structure(s) [30, 31], the extent to which gas-phase

Correspondence to: David Russell; *e-mail:* russell@chem.tamu.edu

ion structures correlate to solution-phase structures is largely unknown.

ESI is an excellent choice for studies of biomolecules because ions are generated directly from solution and the initially generated ions have low internal energies. Beauchamp et al. proposed that the ESI produces ions by a "freeze-dried" mechanism (i.e., in the final stages of ion formation the ions are cooled by solvent evaporation to temperatures of 130–150 K [32]). It is important to recognize, however, that these ions are subsequently warmed by collisions in heated capillaries and/or by collisions with background gas as they traverse the IM and MS analyzers.

Here, we show that the correlation of gas- and solution-phase structures has a significant dependence on changes in the ion's internal energy (E_{int}) that occur following ion formation. Ubiquitin is an excellent model for investigating the effects of E_{int} on ion mobility CCS because it has been extensively studied, both in solution and gas phase as well as by explicit solvent MD simulations [33]. Clemmer et al. noted that ubq^{6+} and ubq^{7+} ions have CCSs that are similar to the native fold [34], and collisional heating of the ions promotes unfolding [35]. Wyttenbach and Bowers also showed that ubiquitin ions formed by ESI from solutions that stabilize the native state were tightly folded solvent-free ions that have CCS that match the sizes of the native state [36]. The extensive database of the conformer preference of solution-phase ubiquitin and the prior folding/unfolding studies of gas-phase ions provide the foundations for our discussion of the dependence of the experimental CCS on E_{int}. In addition to an ordered protein, an intrinsically disordered and less studied protein, human apo-metallothionein-2A (MT) [37, 38], was selected for this investigation. ApoMT, a small metal-binding protein that is similar in size to ubiquitin [37], does not exhibit specific secondary/tertiary structural features, but the metalated form assumes increased order as the number of metal ion bound increases [38–40].

IM-MS and molecular dynamics (MD) simulations are employed to address the question — How closely related are the conformations of ions sampled by IM-MS to the "native structures" of the solution-phase protein ions? The experiments reveal specific effects of various instrumental parameters on CCS. Although this study is limited to the traveling wave (TW) IM-MS instrument (Synapt G2 HDMS) [41], the results are applicable to all IM-MS instruments. The results clearly show that unintended collisional heating alters the E_{int}, and that such changes in E_{int} have strong effects on the conformational diversity as evidenced by changes in the IM CCS; however, careful attention to instrument tuning minimizes these effects and "native-like" conformers can be retained. The experimental data are compared with data obtained by MD simulation at different temperatures, which provides insights into the extent of retention of solution phase structures by IM-MS.

Experimental

Sample Preparation

Bovine ubiquitin (Sigma-Aldrich, St. Louis, MO, USA) was reconstituted to 10 µM in 50 mM ammonium acetate (pH 7.4). ApoMT sample (Bestenbalt LLC, Tallinn, Estonia) was reconstituted to 7 µM using 50 mM ammonium acetate (pH 7.4) solution containing 1 mM Tris(2-carboxyethyl)phosphine hydrochloride (TCEP-HCl; Thermo Fisher Scientific, Rockford, IL, USA) [29, 42]. Metalated Cd_iMT (i = 1 − 7) were obtained by sequential addition of 1, 2, 3, 4, 5, 6, and 7 µL of 1 mM of Cd^{2+} to 100 µL of a 7 µM apoMT solution. Care was taken in all ESI-IM-MS experiments reported here to exclude ESI-induced protein oxidation and nonspecific metal binding as previously described [29, 42].

Ion Mobility-Mass Spectrometry

The ESI IM-MS experiments were performed on a Waters Synapt G2 HDMS instrument (Manchester, UK). "Native state" ESI conditions (H_2O, buffered at pH ~7.4 by using 50 mM ammonium acetate) were used for the studies described below, and the solutions containing the proteins were directly infused into the mass spectrometer at a 0.5 µL/min flow rate. ESI-MS spectra were acquired in the positive ion mode with a capillary voltage of $1.0 - 1.5$ kV. The effects of the changes to voltages applied to the sampling cone (SC), extraction cone (EC), and trap bias (TB), as well as gas flow rates to the He cell and TW analyzer (N_2) on the CCS profiles (see Figure 1a for schematic of the Synapt G2 HDMS instrument) were investigated. These changes are reported in terms of gas flow rates rather than absolute gas pressure because the instrument is not equipped with accurate pressure measurement capabilities. If more accurate pressure measurement capabilities were incorporated, then more detailed studies of how pressure and gas composition affects collision cross section would be possible. A TW velocity of 550 m/s and TW height of 25 V were used for the ubiquitin experiments and 300 m/s and 20 V for MT experiments. All mass spectra were calibrated externally using a solution of sodium iodide. CCS were calibrated using solutions of myoglobin, cytochrome c, and ubiquitin as previously described [43].

Molecular Dynamics Simulations

The NMR structure of ubiquitin (PDB: 1D3Z) and that of separate α and β domains of human MT-2A (1MHU and 2MHU) [37] were used as starting structures for MD simulations. A complete description for MD simulations and parameters for Cd^{2+} ion were described previously [29]. The initial structures were energy-minimized, followed by simulations in vacuo or by implicit solvent model. To mimic the inherent dehydration in the ESI process, the solution-phase structures were subsequently energy-minimized in vacuo to generate "dehydrated structures" [23, 44–46]. To evaluate the protein conformational change caused by ion heating by the IM-MS
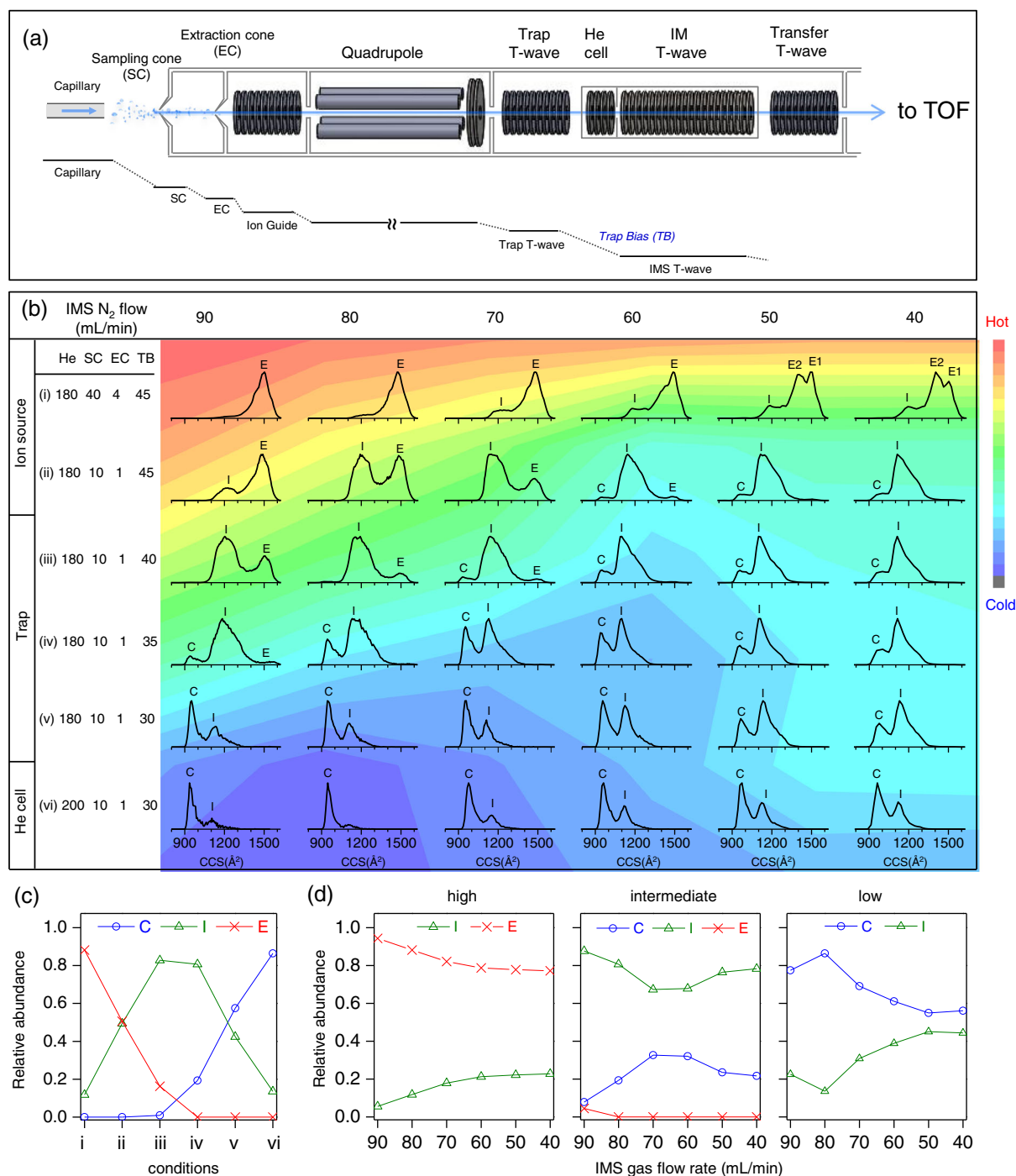
Figure 1. Effects of changes in ion's E_{int} on the CCS profiles. (**a**) Schematic of the Synapt G2 HDMS instrument showing the major parameters that affect ion's E_{int} evaluated in this study and the potential gradient along the instrument. (**b**) CCS profiles for ubq^{6+} ions acquired using a range of instrumental tuning conditions specified in (**a**). Conditions (**i**)–(**vi**) are parameters that are applied prior to the TW-IMS N_2 analyzer. Specifically, the CCS profiles were acquired by varying helium flow rate to the He chamber positioned at the entrance to TW mobility separator, the voltages applied to the individual ion focusing elements (SC, EC, and TB) that are used to guide the ions from the ESI emitter tip to the entrance of the TW mobility separator. SC refers to the ESI skimmer cone, EC denotes the extraction cone, and TB denotes the trap bias lens. Columns 1 – 6 display the effects of N_2 gas flow within the TW mobility separator, and the range of flow rates is noted across the top of (**b**). The color shading of the CCS profiles are intended to show the transition in E_{int} sampled by the specified instrument tuning conditions, where E_{int} decreases on going from red to blue. The changes in the relative abundance of the conformational states [compact (C), intermediate (I), and extended (E)] of ubq^{6+} are plotted in (**c**) for a constant TW N_2 flow rate (80 mL/min), while the electric fields and He flow rate are changed across parameters (**i**)–(**vi**). Similar plots shown in (**d**) were obtained at parameters (**i**), (**iv**), and (**vi**), while varying the N_2 flow rate to the TW analyzer. The temperature map was generated to illustrate the extent of ion heating for each experimental condition (see Experimental section)

spectrometer, simulations with increasing temperature were performed. A detailed procedure for simulation is provided in the Supplementary Material. The simulated structures were clustered using a Cα root mean square deviations (RMSD)-based clustering algorithm in MMTSB tool set [47]. Representative structures, determined as those closest to the centroid of each cluster, were used to represent the candidate experimental structures.

Temperature Maps

The temperature map (Figure 1b) for ubq^{6+} ions was estimated from the range of experimental CCS that were decomposed into multiple conformational families (compact: **C**; intermediate: **I**; and extended: **E**) using Origin v8 (OriginLab Corp., Northampton, MA, USA). The best fit to the experimental peak profiles was obtained using six peaks (see Supplementary Figure S1). The abundances of individual conformations were determined by calculating the area under the peaks. Changes in the abundances of each conformer clearly evident on ion internal energy were then compared with temperature-dependent MD simulations. A strong correlation was obtained between temperature and the value of CCS for the simulated trajectories (i.e., conformers **C**, **I**, and **E** are produced at different temperatures (see Results section). Therefore, the temperature for each experimental condition was estimated using "abundance-weighted" CCS that are calculated on the basis of the relative population of the **C**, **I**, and **E** conformers.

Results

IM-MS of Ubiquitin (ubq^{6+}) Ions

"Native state" ESI of ubiquitin yields predominately the [ubq + 6H]$^{6+}$ (ubq^{6+}) ion (relative abundance >75% abundance; Supplementary Figure S1). CCS profiles for ubq^{6+} ions obtained using a range of instrument parameters (see Figure 1a) are shown in Figure 1b. Although the following discussion is limited to ubq^{6+}, data for ubq^{7+} ions are very similar to that for ubq^{6+} ions (see Supplementary Figure S2). Note that most of the CCS profiles are broad and composed of multiple unresolved signals indicative of an ion population that is composed of multiple conformers. Changes in the CCS profiles as a function of instrument tuning clearly show that conformational changes are occurring post-ESI, but the conformational changes are not reflected in the ESI charge state distribution. For convenience, the CCS profiles are divided into three conformer families: compact (**C**: CCS ~880 to ~1000 Å^2), intermediate (**I**: ~1050 to ~1350 Å^2), and extended state (**E**: ~1400 to ~1600 Å^2), but it should be noted that each family is composed of overlapping/unresolved peaks indicating the presence of multiple similar conformers. For example, two distinct **E** conformations [CCS ~1500 Å^2 (E1) and ~1400 Å^2 (E2)] were observed for N$_2$ flow rates of <50 mL/min of the condition (**i**) (Figure 1b).

The CCS profile shown in row (**i**) of column 1 (Figure 1b) was acquired using the manufacturer's default parameter, which affords the highest ion transmission and detection sensitivity, and it is clear that this condition yields the highest abundance of ions corresponding to the **E** state. The CCS profiles in each column reveal a significant dependence on the electric field and He flow. For example, high SC and EC favor the extended conformer **E**, and reducing these potentials yields appreciable abundances of **I** [see (**i**)–(**ii**)]. The effect of TB is illustrated by comparing the data contained in (**iii**)–(**v**), where the most abundant conformers shift from **I** to **C** as TB is varied from 45 to 30 V. The effects of changing the flow rate of He to the He cell are illustrated in (**vi**). For example, using the same conditions as in (**v**) but increasing the He flow to the maximum (200 mL/min) yields predominately **C**. A quantitative plot that illustrates the effects of the electric fields and the gas (He) flow rate to the He cell is represented in Figure 1c, which shows the abundances for the three conformer families (**E**, **I**, and **C**) at a fixed IMS gas (N$_2$) flow rate (80 mL/min) as a function of parameters for (**i**) − (**vi**). Note that these parameters result in changes in E$_{int}$ prior to the ions entering the TW IMS analyzer. The results show that the sequential decrease of electric field and an increase in He flow [from conditions (**i**) to (**vi**)] favors more compact conformers.

The CCS profiles also show a significant dependence on the N$_2$ gas flow rate, which can be seen by comparing the profiles in each row as the N$_2$ flow rate to the TW analyzer is reduced from 90 to 40 mL/min. For example, as the N$_2$ flow rate is reduced from 90 to 40 mL/min the profiles in row (**i**) shift to smaller CCS, transitioning from **E1** to **E2** and finally to **I**. The quantitative data showing changes in the CCS profiles as a function of N$_2$ flow rate to the TW separator are shown in Figure 1d. Here, the abundances of **C**, **I**, and **E** are plotted for various N$_2$ flow rates obtained using instrument tuning parameters that favor high, intermediate, and low electric fields, conditions (**i**), (**iv**), and (**vi**) in Figure 1b, respectively. As noted above, conformer(s) **E** dominates the CCS profiles taken using high electric fields and decreasing the N$_2$ flow rate causes a reduction in **E** with a concomitant increase in the abundance of **I**. The data obtained using intermediate electric fields [i.e., those used for condition (**iv**)], are dominated by **I** and the abundances of **C** and **E** are lower at N$_2$ flow rates of 90 mL/min, and changing the flow rate (80 − 70 mL/min) results in an increase in **C** and decreases in both **I** and **E**. The abundances of **C** and **I** do not change significantly for N$_2$ flow rates of 70 − 60 mL/min, and further decrease in the flow rate (<60 mL/min) results in an increase in **I** and concomitant decrease in **C**. Lastly, the data collected at low electric fields [row (**vi**)] show that **C** is favored at N$_2$ flow rates of 90 − 80 mL/min but the ion population is shifted to **I** at low gas flow rates.

IM-MS of Human MT-2A

CCS profiles for apoMT and the partially- and fully-metalated states (Cd$_i$MT^{5+} i = 0 − 7) are shown in Figure 2. We previously showed that addition of Cd^{2+} to MT promotes folding as
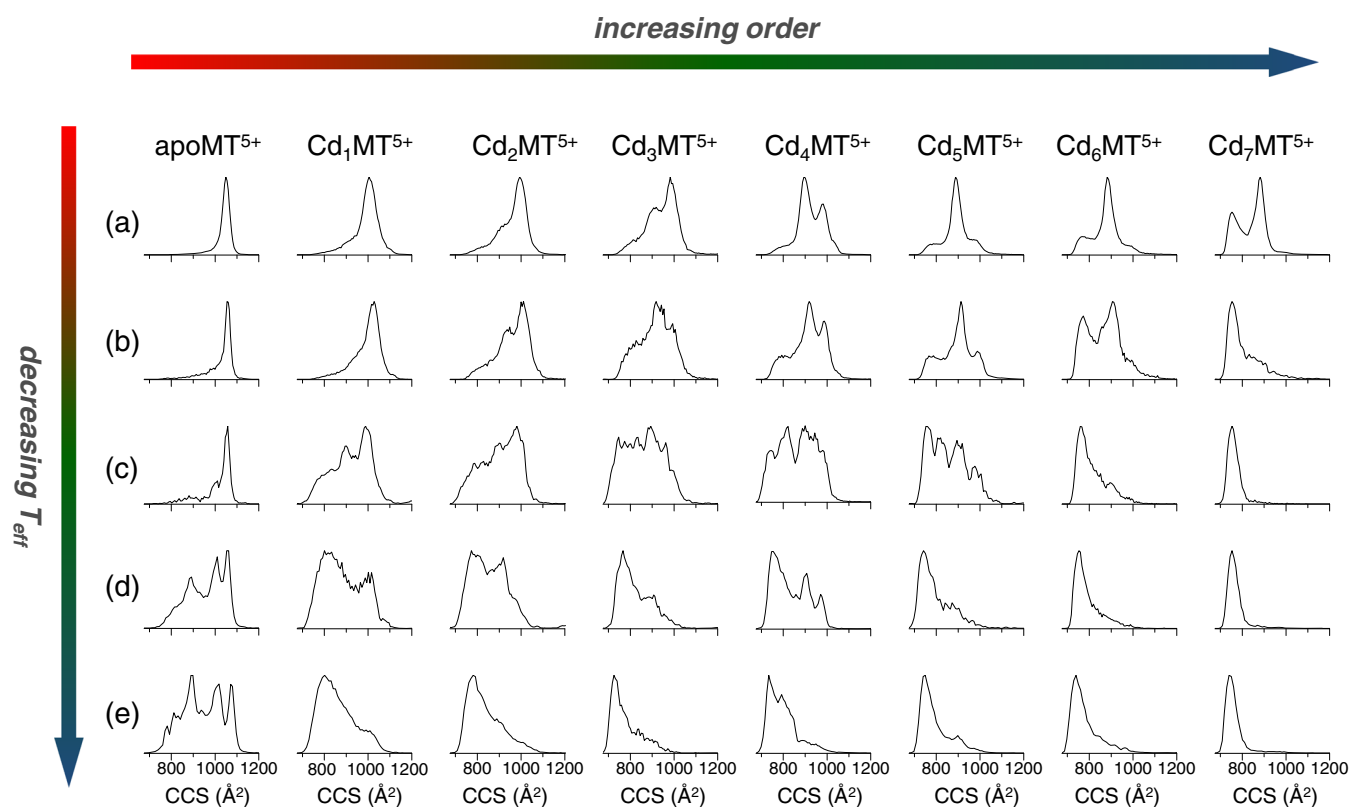
Figure 2. Ion mobility profiles of Cd_iMT (i = 0 – 7) acquired under various instrument conditions. The voltages of sampling cone (SC), extraction cone (EC), trap bias (TB), and flow of He and IMS cell were: (**a**) 60 V, 4 V, 45 V, 180, and 90 mL/min, (**b**) 10 V, 1 V, 45 V, 180, and 90 mL/min, (**c**) 10 V, 1 V, 35 V, 180, and 90 mL/min, (**d**) 10 V, 1 V, 35 V, 180, and 70 mL/min, and (**e**) 10 V, 1 V, 35 V, 200, and 70 mL/min, respectively

evidenced by increase in the abundances of compact conformers as the number of bound metal ions increases [29]. In that paper, we only reported CCS data for the Cd_iMT ions (i = 0–7) that were obtained using instrument parameters that correspond to a low E_{int} condition [29]. The data shown in Figure 2 span the similar range of instrument tuning parameters as discussed above for ubq^{6+} ions. The effects of E_{int} can be seen by comparing the CCS profiles in rows (a) − (e) in Figure 2. That is, (a) reports CCS data for ions having high E_{int} and high ion transfer efficiencies and (e) corresponds the condition where lowest E_{int} is achieved. As expected, the condition (a) favors an ion population composed exclusively of extended conformers; however, CCS profiles collected at progressively lower E_{int} (going down each column) contain partially resolved conformers or conformer families that are relatively compact. It is interesting to note that the CCS profile for apoMT remains highly heterogeneous at the lowest E_{int}, which is further evidence that the protein is indeed best described as an IDP. Similar broad, multi-component CCS profiles are observed for the partially metalated ions, especially for i = 1–5. We note that the CCS transition collected using the lowest E_{int} [row (e)] corresponds to a transition from disordered to ordered conformation, which is consistent with solution studies [38–40]. That is, as the number of Cd^{2+} ions increases, there are significant changes in the CCS profiles owing to diminution in the

conformer population as well as shift to small values in their respective CCS. On the other hand, the effect of binding of metal ions on the sensitivity of the CCS transition can be seen by comparing the data between the columns, viz. as i increases, greater energy input is required to unfold Cd_iMT.

Molecular Dynamics Simulation of Ubiquitin and Cd_iMT (i = 0–7)

Implicit water and in vacuo MD simulations were used to generate candidate conformations of ubiquitin and apo-, partially-, and fully-metalated MT ions. Solution-phase structures are then subjected to in vacuo energy minimization to generate dehydrated structures [22, 44–46]. Simulations for 300 K gas phase and dehydrated ubq^{6+} ions over a 10-ns window yield globular conformations (Supplementary Figure S3). The dehydrated ions retain solution-phase secondary structure elements, whereas the secondary structure elements of the gas-phase ions are somehow disrupted. That is, a higher degree of helix and β-sheet structure is retained in the dehydrated conformers than is observed for the gas-phase ions (see Supplementary Figure S3). Regardless, the average CCS of the gas- and solution-phase conformers are quite similar, 921.7±6.1 Å^2 and 934.0±10.1 Å^2, respectively, and both are in reasonable agreement with the experimental value for the compact **C** conformers.
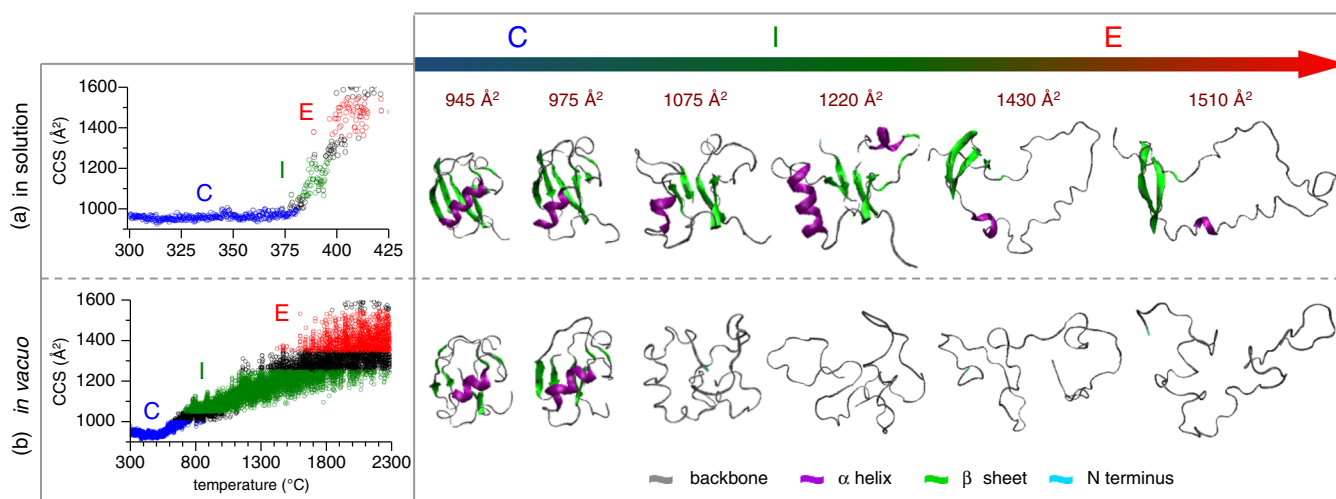
Figure 3. Simulations of the effect of temperature on (**a**) dehydrated and (**b**) gas-phase ubiquitin structure. Dehydrated structures are generated by in vacuo minimization of solution structures that underwent thermal unfolding in the presence of water; gas phase structures are simulated in the absence of water

Temperature-dependent conformations for solution and in vacuo simulations of ubiquitin ions are shown in Figure 3a and

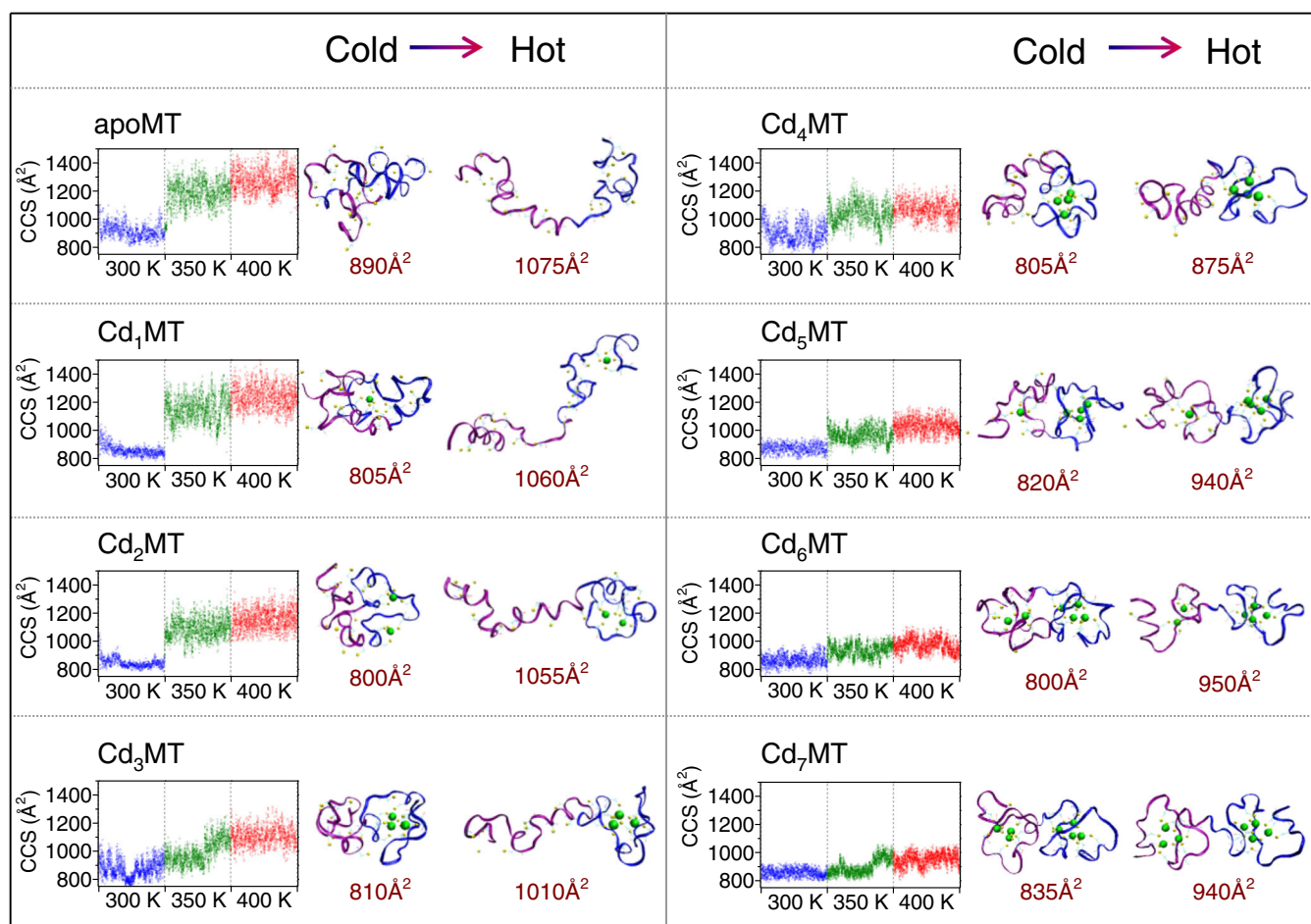b, respectively. The solution simulations were designed to mimic heating that occurs while water molecules are still

Figure 4. MD simulations of *dehydrated* $Cd_i MT$ (i = 0 − 7) at temperatures of 300, 350, and 400 K. The time window for each temperature is 5 ns. Similar simulation data for *gas phase* $Cd_i MT$ (i = 0 − 7) under thermal unfolding is provided in Supplementary Information Figure S4

attached to the ions in ESI (Figure 3a); however, the simulations do not account for the evaporative cooling that may accompany droplet evaporation [32]. The calculated CCS for the solution dehydrated structures over the range of temperatures from 300 to ~375 K fall within the range of the compact conformer $\mathbf{C}$ (~950 Å^2), and as the temperature is increased, the CCS transition through $\mathbf{I}$ (~1200 Å^2) and eventually to $\mathbf{E}$ (~1500 Å^2). Figure 3b contains similar data for gas-phase unfolding in a solvent-free environment, viz. representative of ion heating in late stages of ESI as well as any changes in E_{int} as the ions traverse the regions of the instrument that guide the ions to the TW analyzer. Note that ions from gas-phase unfolding have a very different dependence on temperature than do the solution-phase ions. As temperature increases from ~300 to 500 K, the protein undergoes some compaction with a small loss of 2° structure elements, but the changes in CCS are small, ~3%. Further increase in temperature (>600 K) results in complete loss of 2° structure elements resulting in formation of largely disordered conformations. Specifically, the temperature to unfold gas-phase ions is much higher than that for solution-phase ions, and the structural heterogeneity is also much greater for unfolded gas phase ions.

The gas phase, hydrated, and dehydrated candidate structures for the various Cd$_i$MT species were generated as described above for ubiquitin [29]. Unlike ubiquitin, MT is disordered in solution, and thus the structural evolution at fixed temperatures was evaluated. Figure 4 shows the time-dependent CCS and representative conformations for dehydrated Cd$_i$MTs at temperatures of 300, 350, and 400 K. The simulation data show a good agreement with the experimental CCS and both of them suggest that (1) at 300 K the protein disorder decreases as the numbers of Cd^{2+} ions bound increases, (2) the protein unfolds as temperature increases independent of the numbers of Cd^{2+} ions bound, and (3) the transition in CCS for apoMT (disordered protein) is much more sensitive to temperature compared with that of Cd$_7$MT (ordered protein). For example, at 300 − 350 K a sharp transition from the compact conformer (CCS ~890 Å^2) to a partially-unfolded conformer (CCS ~1100 to 1200 Å^2) is evident for i = 0–2, but similar transitions are less apparent for the i = 3–7 ions; however, there is an overall increase in CCS as temperature increases. Note similar simulation data for the gas-phase unfolding of Cd$_i$MT are provided in Supplementary Figure S4, and these data clearly show similar unfolding transition as the temperature increases.

Discussion

Heck defines "native-state ESI" as the ability to retain quaternary structure of the biomolecule complex [17], and Ruotolo et al.'s studies on the collision-induced unfolding (CIU) of small molecules bound to proteins and protein complexes provide additional support for Heck's definition [48]. That is, at low E_{int} the complexes have smaller CCSs than do complexes that have been subjected to CIU. Similarly, the

experimental CCS profiles for ubq^{6+} and Cd$_i$MT^{5+} (i = 0 − 7) ions produced by using native-ESI conditions and then examined at the lowest possible E_{int} by IM-MS have CCSs that agree with those for solution-phase structures. When these same ions are sampled using conditions corresponding to increased E_{int}, which promote unfolding of the gas-phase ions, their CCSs are in excellent agreement with CCSs for candidate structures obtained from the temperature-ramped MD simulations.

The data for ubq^{6+} and Cd$_i$MT^{5+} clearly show changes in the conformer distributions as the solvent-free ions traverse the instrument between the ESI source and the TW analyzer. Although it should be noted that proteins/ions that have the same CCS may not have identical structures (i.e., it is possible that the conformational population observed in IM-MS is the result of slow gas phase refolding processes [49, 50]), the CCS profiles for ions that have the lowest E_{int} [Figure 1b, columns 1 and 2, row (**vi**)] clearly show that these ions have CCSs that resemble the native fold, providing good evidence that the low E_{int} conditions used for this study produce an ion population that is primarily "native." Note the CCS for $\mathbf{C}$ is in excellent agreement with that of the "native-state" CCS for the NMR structure (see Supplementary Figure S3) and that reported by Clemmer, Bowers, and coworkers [34, 36]. Thus, changes in the conformer distribution that are reflected by changes in the CCS profiles must be related to changes in E_{int} that occur post-ESI, viz. energetic ion-neutral collisions as the ions are guided by focusing devices from the ion source to the TW analyzer. Previous studies by DePauw, Williams, and coworkers clearly show that the internal energies of small thermometer ions are sensitive to the TW velocity and amplitude [51–53]; however, the CCS profiles for the protein ions studied here do not show significant dependence on the tuning of the TW analyzer (see Supplementary Figure S5). The differences between small and large molecule ions may be attributed to the number of degrees-of-freedom into which energy can be channeled [54]; thus, the effects of changes in E_{int} are expected to be much less for large molecule ions. In addition, conformers that are stabilized by intramolecular interactions may better retain solution-phase structural features. Although our data clearly show that SC, EC, TB, He, and N$_2$ flow rates have marked effects on E_{int} for protein ions, we do not find any evidence that ion source temperature or tuning of the TW Trap ion guide (flow rate of Ar and wave height and velocity) have any significant effects on E_{int}.

The temperature map that is superimposed on the ubq^{6+} ion CCS profiles clearly shows that changes in SC, EC, TB, and He flow shift the conformer preferences from $\mathbf{E} \rightarrow \mathbf{I} \rightarrow \mathbf{C}$ as ions having lower E_{int} are sampled. Note that the decrease in these potentials and the increase in the flow rate of He significantly reduce the kinetic energy of ions before they enter the N$_2$ (IMS) cell, thereby resulting in decreases in E_{int}. The overall trends in the data indicate that the ion population generated by "native-state ESI" can be preserved under conditions of low E_{int}. Further, the temperature map also illustrates an intricate interplay between E_{int} and the N$_2$ gas flow rate within the TW analyzer, viz. the distribution of conformers can be altered by

energetic collisions that occur within the TW analyzer. The CCS profiles in the first column of the temperature map (Figure 1b) are a direct measure of the conformer distribution as it enters the TW analyzer, and any changes in the conformer distribution that arise as the N_2 gas flow rate is decreased are a result of cooling/heating by collisions in the TW analyzer. For example, row (**i**) shows the results of cooling the ion population introduced to the TW analyzer by using the manufacturer's "default" settings for SC, EC, and TB. Reducing the N_2 flow rate is accompanied by a decrease in the relative abundance of **E** and a corresponding increase in **I** owing to a reduction in E_{int}. At the other extreme, row (**vi**), the initial ion population is composed primarily of "native" state ubq^{6+} ions, and decrease in the N_2 flow rate results in an increased abundance of higher energy conformers owing to increased E_{int} relative to the initial E_{int} for the ions that enter the TW analyzer. In summary, ions entering the TW analyzer with high E_{int} are cooled as the ratio of N_2 is reduced, whereas ions entering the TW with low E_{int} are heated under these same conditions. The data in rows (**ii**) − (**v**) show that under these conditions, ion's E_{int} initially decreases and then increases. Note that the CCS profiles along the diagonal from bottom-left to top-right appear to correspond to tuning conditions that favor the lowest E_{int} for each row (Figure 1b). This observation raises important questions—Why does the flow rate of N_2 have such a dramatic effect on conformer distribution—how do decreases of N_2 flow achieve opposite effects (cooling or heating) that are dependent on initial conditions? First, using high flow rates of N_2, the He leak rate (into N_2 TW cell) will be small, but it will increase as the N_2 flow rate is reduced. Under the conditions of reduced N_2 flow rate, the ratio of He/N_2 in the TW analyzer increases, and the increased partial pressure of the lighter collision partner (He) reduces energy transfer by the ion-neutral collisions [54]. Second, the mean-free-path of ions within the IMS cell increases as the flow of N_2 is reduced, thus increasing the kinetic energy gained by each collision event. Note that the combination of these two effects determines the E_{int} of the ions. In our experiments, using strong ion focusing conditions [row (**i**)], ions acquire substantial kinetic energy prior to entering the IMS cell and this large kinetic energy is converted into internal vibrational energy or E_{int} by energetic collisions at the entrance of the IMS cell, which dominates the overall E_{int} of the ions; however, the ions are cooled as the ratio of He/N_2 increases (N_2 is varied from 90 to 40 mg/mL). In cases of low electric fields [row (**vi**)], where ions do not acquire appreciable amounts of kinetic energy prior to entering the IMS cell, the increase in E_{int} at the entrance of the TW analyzer is expected to be relatively small, and thus the overall E_{int} is dominated by the slow heating due to the increased mean-free-path within the IMS cell. As expected, the changes of E_{int} at the intermediate electric fields [row (**iv**)] are governed by both factors.

Unlike ubiquitin, apoMT is disordered in solution, but the effects of changes in E_{int} are quite similar. That is, the CCS profiles for $apoMT^{5+}$ (first column of Figure 2) clearly show that an extended conformation is favored at the highest E_{int}; however, decreasing E_{int} (top-to-bottom, first column) shifts

the CCS profile and produces partially resolved peaks, indicative of an ion population that is composed of multiple conformer families. In addition, the CCS profiles for the partially- and fully-metalated Cd_iMT ions are shifted owing to a higher degree of order as metal ions are added (from left-to-right for each row, Figure 2). The increased conformational order is a direct result of strong metal–thiolate binding that stabilizes the protein structure. The E_{int}-dependent conformer distribution was observed for the metalated forms. For example, the CCS profile for the highly ordered Cd_7MT^{5+} ion is multi-component even at high E_{int}, but it eventually converges to a single compact conformer (bottom row of column 8). Similar trends are also observed for all partially-metalated forms.

Although all of the Cd_iMT^{5+} ions unfold as E_{int} is increased, their E_{int}-dependent unfolding is quite different. For example, Cd_7MT^{5+} maintains the native-like fold at medium E_{int} [condition (**c**)] but under the same conditions the $apoMT^{5+}$ is significantly activated and composed of a single elongated conformation (Figure 2). This differential E_{int}-dependent unfolding observed for $apoMT^{5+}$ and Cd_iMT^{5+} ions is attributed to differing degrees of stabilization by intramolecular interaction (i.e., the presence of strong metal–thiolate interaction introduced by the binding of metal ion makes protein ions more resistant to ion heating.

There are two potential approaches that can be used to probe folding/unfolding pathways of gas phase ions as a function of E_{int} and or time: (1) IM-MS [35, 55, 56] and (2) electron-capture dissociation (ECD) combined with hydrogen/deuterium exchange (HDX) [50, 57, 58]. Here, MD simulations are used to generate temperature-dependent conformer preferences [59, 60]. The data contained in Figure 3 illustrate that ion heating in water and in the gas phase gradually depletes the protein 2° and 3° structures, and these processes form multiple intermediates that involve formation of the elongated conformers. However, the unfolding pathways are distinct between the two models: (1) the partially unfolded **I** conformers differ significantly, viz. the dehydrated structures retain the 2° structures of the native fold for a longer period of time, whereas these interactions are disrupted very quickly for the gas-phase ions; (2) the unfolding in gas-phase ions proceeds much more slowly and results in a much broader dispersion in CCS, probably owing to the strong intramolecular electrostatic interaction (charge solvation) in the absence of water.

The simulated temperature-dependent conformer preferences are consistent with the experimental data. That is, a structural transition from compact to extended conformations is observed for both ubq^{6+} and Cd_iMT^{5+} ions; however, it should be noted that the simulation data presented here only represent possible unfolded conformations and possible unfolding pathways. It is also noted that there may be many possible parallel pathways to the energetically accessible unfolded states [57, 58].

The E_{int}-dependent conformational changes provide important insights into the protein energy folding landscape. To date, very little is known about the effects of metalation on folding/

unfolding of metalloproteins [38]. The solution-phase-like conformational landscape is best represented by the CCS data collected with minimal energy perturbation. For example, the CCS data for apoMT is consistent with that of an intrinsically disordered protein (IDP) (i.e., an energy folding landscape composed of multiple energy minima). Addition of metal ions converge the distinct conformations to a narrow CCS profile, which can be correlated to changes in the folding landscape (i.e., metal binding induces new structural domains, thereby reducing the flexibility of the molecule). Such changes result in narrowing of the conformational space and deepening of the funnel-shaped landscape. As the number of metal ions bound increases, the depth of the funnel increases, in line with the E_{int}-dependent data shown in Figure 2. For example, the CCS profile for Cd_7MT^{5+} appears to be unchanged over the range of conditions used to acquire (c) − (e); however, that of $apoMT^{5+}$ has changed dramatically when the same range of conditions is used. The E_{int}-dependent data for the partially metalated ions, Cd_iMT^{5+} (i = 1–6), clearly show that distinct CCS profiles are obtained using specific instrument tuning conditions that yield either low or high E_{int} ion populations; however, changes in the CCS profiles are observed as the ion's E_{int} is either increased (collisional activation) or decreased (collisional cooling). Such changes in the E_{int} allow the ions to sample different regions of the energy folding landscape corresponding to gas-phase folding/unfolding reactions.

Conclusions

"Native mass spectrometry" is emerging as a powerful technology in structural biology, and experimental parameters that most strongly affect "Native ESI" are now quite well defined [17]; however, the question how "native" are ions sampled by the IMS experiment remains elusive. That is, there is considerable time lag (10–100 μs) between ion formation and ions entering the IMS analyzer, and the ions can unfold/refold on this time scale [49]. Also, collisional activation can occur as ions are guided/focused by electrostatic lens and ion-neutral collision as they travel from the ion source to the IMS analyzer, and E_{int} can also be increased by black-body irradiation from their surroundings [61]. Clearly, increases in E_{int} influence protein conformation, and thus to what extent does the journey from source to IMS analyzer influence conformer preferences of large molecule ions, how do these effects influence IMS data, and most importantly, can we correlate "native" and "non-native" states sampled by IM-MS to solution "native" conformation?

Here, we clearly show that IMS CCS profiles do not always retain the structural feature for the "native" structure when the ions are formed using "native-ESI" conditions. In cases of large proteins or protein complexes, the available experimental data support the claims that solution-phase structural features are retained; however, TW IMS studies for ubq^{6+} ions [53] and drift tube IMS for $apoMT^{5+}$ [62] show that they adopt extended conformations that differ significantly from the native-like state; however, data shown in the current study clearly indicate

that under conditions that minimize E_{int}, the CCS profiles are consistent with the results reported by solution studies, for both ordered (ubiquitin, Cd_7MT) and disordered (apoMT) proteins.

This study serves as a cautionary note for interpreting structural information and careful evaluation of the experimental IM-MS parameters prior to assignments of ion conformation. In these studies, the conformational changes associated with 2° and 3° structure that are occurring as the ions traverse the instrument are derived from cumulative effects of individual ion focusing optics. On the other hand, the data suggest that careful tuning of instrumental parameters allows preservation of native-like conformation. This study also helps to define specific tuning guidelines that achieve low E_{int} for the most widely used IM-MS instrument for protein structure and structural biology.

Acknowledgments

References

1. Chiti, F., Dobson, C.M.: Protein misfolding, functional amyloid, and human disease. Annu. Rev. Biochem. **75**, 333–366 (2006)
2. Wright, P.E., Dyson, H.J.: Intrinsically unstructured proteins: reassessing the protein structure-function paradigm. J. Mol. Biol. **293**, 321–331 (1999)
3. Dunker, A.K., Lawson, J.D., Brown, C.J., Williams, R.M., Romero, P., Oh, J.S., Oldfield, C.J., Campen, A.M., Ratliff, C.M., Hipps, K.W., Ausio, J., Nissen, M., Reeves, R., Kang, C., Kissinger, C.R., Bailey, R.W., Griswold, M.D., Chiu, W., Garner, E.C., Obradovic, Z.: Intrinsically disordered protein. J. Mol. Graph. Model. **19**, 26–59 (2001)
4. Chouard, T.: Structural biology: breaking the protein rules. Nature **471**, 151–153 (2011)
5. Uversky, V.N., Dave, V., Iakoucheva, L.M., Malaney, P., Metallo, S.J., Pathak, R.R., Joerger, A.C.: Pathological unfoldomics of uncontrolled chaos: intrinsically disordered proteins and human diseases. Chem. Rev. **114**, 6844–6879 (2014)
6. Uversky, V.N., Oldfield, C.J., Dunker, A.K.: Intrinsically disordered proteins in human diseases: introducing the D2 concept. Annu. Rev. Biophys. **37**, 215–246 (2008)
7. Iakoucheva, L.M., Brown, C.J., Lawson, J.D., Obradovic, Z., Dunker, A.K.: Intrinsic disorder in cell-signaling and cancer-associated proteins. J. Mol. Biol. **323**, 573–584 (2002)
8. Dyson, H.J., Wright, P.E.: Intrinsically unstructured proteins and their functions. Nat. Rev. Mol. Cell Biol. **6**, 197–208 (2005)
9. Dyson, H.J., Wright, P.E.: Elucidation of the protein folding landscape by NMR. Methods Enzymol. **394**, 299–321 (2005)
10. Kwan, A.H., Mobli, M., Gooley, P.R., King, G.F., Mackay, J.P.: Macromolecular NMR spectroscopy for the non-spectroscopist. FEBS J. **278**, 687–703 (2011)
11. Konermann, L., Pan, J., Liu, Y.H.: Hydrogen exchange mass spectrometry for studying protein structure and dynamics. Chem. Soc. Rev. **40**, 1224–1234 (2011)
12. Keppel, T.R., Weis, D.D.: Analysis of disordered proteins using a simple apparatus for millisecond quench-flow H/D exchange. Anal. Chem. **85**, 5161–5168 (2013)
13. Keppel, T.R., Weis, D.D.: Mapping residual structure in intrinsically disordered proteins at residue resolution using millisecond hydrogen/deuterium exchange and residue averaging. J. Am. Soc. Mass Spectrom. **26**, 547–554 (2015)
14. Apuy, J.L., Chen, X., Russell, D.H., Baldwin, T.O., Giedroc, D.P.: Ratiometric pulsed alkylation/mass spectrometry of the cysteine pairs in

individual zinc fingers of MRE-binding transcription factor-1 (MTF-1) as a probe of zinc chelate stability. Biochemistry **40**, 15164–15175 (2001)

15. Apuy, J.L., Busenlehner, L.S., Russell, D.H., Giedroc, D.P.: Ratiometric pulsed alkylation mass spectrometry as a probe of thiolate reactivity in different metalloderivatives of *Staphylococcus aureus* pI258 CadC. Biochemistry **43**, 3824–3834 (2004)

16. Gau, B.C., Sharp, J.S., Rempel, D.L., Gross, M.L.: Fast photochemical oxidation of protein footprints faster than protein unfolding. Anal. Chem. **81**, 6563–6571 (2009)

17. Heck, A.J.: Native mass spectrometry: a bridge between interactomics and structural biology. Nat. Methods **5**, 927–933 (2008)

18. Hernandez, H., Robinson, C.V.: Determining the stoichiometry and interactions of macromolecular assemblies from mass spectrometry. Nat. Protoc. **2**, 715–726 (2007)

19. Lanucara, F., Holman, S.W., Gray, C.J., Eyers, C.E.: The power of ion mobility-mass spectrometry for structural characterization and the study of conformational dynamics. Nat. Chem. **6**, 281–294 (2014)

20. Clemmer, D.E., Hudgins, R.R., Jarrold, M.F.: Naked protein conformations: cytochrome *c* in the gas phase. J. Am. Chem. Soc. **117**, 10141–10142 (1995)

21. Bernstein, S.L., Dupuis, N.F., Lazo, N.D., Wyttenbach, T., Condron, M.M., Bitan, G., Teplow, D.B., Shea, J.E., Ruotolo, B.T., Robinson, C.V., Bowers, M.T.: Amyloid-beta protein oligomerization and the importance of tetramers and dodecamers in the aetiology of Alzheimer's disease. Nat. Chem. **1**, 326–331 (2009)

22. Bernstein, S.L., Liu, D., Wyttenbach, T., Bowers, M.T., Lee, J.C., Gray, H.B., Winkler, J.R.: Alpha-synuclein: stable compact and extended monomeric structures and pH dependence of dimer formation. J. Am. Soc. Mass Spectrom. **15**, 1435–1443 (2004)

23. Bernstein, S.L., Wyttenbach, T., Baumketner, A., Shea, J.E., Bitan, G., Teplow, D.B., Bowers, M.T.: Amyloid beta-protein: monomer structure and early aggregation states of Abeta42 and its Pro19 alloform. J. Am. Chem. Soc. **127**, 2075–2084 (2005)

24. Canon, F., Ballivian, R., Chirot, F., Antoine, R., Sarni-Manchado, P., Lemoine, J., Dugourd, P.: Folding of a salivary intrinsically disordered protein upon binding to tannins. J. Am. Chem. Soc. **133**, 7847–7852 (2011)

25. Pagel, K., Natan, E., Hall, Z., Fersht, A.R., Robinson, C.V.: Intrinsically disordered p53 and its complexes populate compact conformations in the gas phase. Angew. Chem. Int. Ed. Engl. **52**, 361–365 (2013)

26. Jurneczko, E., Cruickshank, F., Porrini, M., Clarke, D.J., Campuzano, I.D., Morris, M., Nikolova, P.V., Barran, P.E.: Probing the conformational diversity of cancer-associated mutations in p53 with ion-mobility mass spectrometry. Angew. Chem. Int. Ed. Engl. **52**, 4370–4374 (2013)

27. Saikusa, K., Fuchigami, S., Takahashi, K., Asano, Y., Nagadoi, A., Tachiwana, H., Kurumizaka, H., Ikeguchi, M., Nishimura, Y., Akashi, S.: Gas-phase structure of the histone multimers characterized by ion mobility mass spectrometry and molecular dynamics simulation. Anal. Chem. **85**, 4165–4171 (2013)

28. Jurneczko, E., Cruickshank, F., Porrini, M., Nikolova, P., Campuzano, I.D., Morris, M., Barran, P.E.: Intrinsic disorder in proteins: a challenge for (un)structural biology met by ion mobility-mass spectrometry. Biochem. Soc. Trans. **40**, 1021–1026 (2012)

29. Chen, S.-H., Chen, L., Russell, D.H.: Metal-induced conformational changes of human metallothionein-2A: a combined theoretical and experimental study of metal-free and partially metalated intermediates. J. Am. Chem. Soc. **136**, 9499–9508 (2014)

30. Ruotolo, B.T., Giles, K., Campuzano, I., Sandercock, A.M., Bateman, R.H., Robinson, C.V.: Evidence for macromolecular protein rings in the absence of bulk water. Science **310**, 1658–1661 (2005)

31. Uetrecht, C., Rose, R.J., van Duijn, E., Lorenzen, K., Heck, A.J.: Ion mobility mass spectrometry of proteins and protein assemblies. Chem. Soc. Rev. **39**, 1633–1655 (2010)

32. Lee, S.-W., Freivogel, P., Schindler, T., Beauchamp, J.L.: Freeze-dried biomolecules: FT-ICR studies of the specific solvation of functional groups and clathrate formation observed by the slow evaporation of water from hydrated peptides and model compounds in the gas phase. J. Am. Chem. Soc. **120**, 11758–11765 (1998)

33. Kony, D.B., Hunenberger, P.H., van Gunsteren, W.F.: Molecular dynamics simulations of the native and partially folded states of ubiquitin: influence of methanol cosolvent, pH, and temperature on the protein structure and dynamics. Protein Sci. **16**, 1101–1118 (2007)

34. Koeniger, S.L., Clemmer, D.E.: Resolution and structural transitions of elongated states of ubiquitin. J. Am. Soc. Mass Spectrom. **18**, 322–331 (2007)

35. Shi, H., Atlasevich, N., Merenbloom, S.I., Clemmer, D.E.: Solution dependence of the collisional activation of ubiquitin $[M + 7H]^{7+}$ ions. J. Am. Soc. Mass Spectrom. **25**, 2000–2008 (2014)

36. Wyttenbach, T., Bowers, M.T.: Structural stability from solution to the gas phase: native solution structure of ubiquitin survives analysis in a solvent-free ion mobility-mass spectrometry environment. J. Phys. Chem. B **115**, 12266–12275 (2011)

37. Messerle, B.A., Schaffer, A., Vasak, M., Kagi, J.H., Wuthrich, K.: Three-dimensional structure of human $[^{113}Cd_7]$metallothionein-2 in solution determined by nuclear magnetic resonance spectroscopy. J. Mol. Biol. **214**, 765–779 (1990)

38. Blindauer, C.A., Leszczyszyn, O.I.: Metallothioneins: unparalleled diversity in structures and functions for metal ion homeostasis and more. Nat. Prod. Rep. **27**, 720–741 (2010)

39. Romero-Isart, N., Vasak, M.: Advances in the structure and chemistry of metallothioneins. J. Inorg. Biochem. **88**, 388–396 (2002)

40. Maret, W.: Redox biochemistry of mammalian metallothioneins. J. Biol. Inorg. Chem. **16**, 1079–1086 (2011)

41. Pringle, S.D., Giles, K., Wildgoose, J.L., Williams, J.P., Slade, S.E., Thalassinos, K., Bateman, R.H., Bowers, M.T., Scrivens, J.H.: An investigation of the mobility separation of some peptide and protein ions using a new hybrid quadrupole/traveling wave IMS/oa-ToF instrument. Int. J. Mass Spectrom. **261**, 1–12 (2007)

42. Chen, S.-H., Russell, W.K., Russell, D.H.: Combining chemical labeling, bottom-up, and top-down ion-mobility mass spectrometry to identify metal-binding sites of partially metalated metallothionein. Anal. Chem. **85**, 3229–3237 (2013)

43. Ruotolo, B.T., Benesch, J.L., Sandercock, A.M., Hyung, S.J., Robinson, C.V.: Ion mobility-mass spectrometry analysis of large protein complexes. Nat. Protoc. **3**, 1139–1152 (2008)

44. Baumketner, A., Bernstein, S.L., Wyttenbach, T., Bitan, G., Teplow, D.B., Bowers, M.T., Shea, J.E.: Amyloid beta-protein monomer structure: a computational and experimental study. Protein Sci. **15**, 420–408 (2006)

45. Dupuis, N.F., Wu, C., Shea, J.E., Bowers, M.T.: The amyloid formation mechanism in human IAPP: dimers have beta-strand monomer-monomer interfaces. J. Am. Chem. Soc. **133**, 7240–7243 (2011)

46. Pierson, N.A., Chen, L., Valentine, S.J., Russell, D.H., Clemmer, D.E.: Number of solution states of bradykinin from ion mobility and mass spectrometry measurements. J. Am. Chem. Soc. **133**, 13810–13813 (2011)

47. Feig, M., Karanicolas, J., Brooks III, C.L.: MMTSB Tool Set: enhanced sampling and multiscale modeling methods for applications in structural biology. J. Mol. Graph. Model. **22**, 377–395 (2004)

48. Hyung, S.J., Robinson, C.V., Ruotolo, B.T.: Gas-phase unfolding and disassembly reveals stability differences in ligand-bound multiprotein complexes. Chem. Biol. **16**, 382–390 (2009)

49. Breuker, K., McLafferty, F.W.: Stepwise evolution of protein native structure with electrospray into the gas phase, 10^{-12} to 10^{2} s. Proc. Natl. Acad. Sci. U. S. A. **105**, 18145–18152 (2008)

50. Schennach, M., Breuker, K.: Proteins with highly similar native folds can show vastly dissimilar folding behavior when desolvated. Angew. Chem. Int. Ed. Engl. **53**, 164–168 (2014)

51. Gabelica, V., De Pauw, E.: Internal energy and fragmentation of ions produced in electrospray sources. Mass Spectrom. Rev. **24**, 566–587 (2005)

52. Morsa, D., Gabelica, V., De Pauw, E.: Fragmentation and isomerization due to field heating in traveling wave ion mobility spectrometry. J. Am. Soc. Mass Spectrom. **25**, 1384–1393 (2014)

53. Merenbloom, S.I., Flick, T.G., Williams, E.R.: How hot are your ions in TWAVE ion mobility spectrometry? J. Am. Soc. Mass Spectrom. **23**, 553–562 (2012)

54. Wells, J.M., McLuckey, S.A.: Collision-induced dissociation (CID) of peptides and proteins. Methods Enzymol. **402**, 148–185 (2005)

55. Myung, S., Badman, E.R., Lee, Y.J., Clemmer, D.E.: Structural transitions of electrosprayed ubiquitin ions stored in an ion trap over ~10 ms to 30 s. J. Phys. Chem. A **106**, 9976–9982 (2002)

56. Badman, E.R., Myung, S., Clemmer, D.E.: Evidence for unfolding and refolding of gas-phase cytochrome C ions in a Paul trap. J. Am. Soc. Mass Spectrom. **16**, 1493–1497 (2005)

57. Breuker, K., Oh, H., Horn, D.M., Cerda, B.A., McLafferty, F.W.: Detailed unfolding and folding of gaseous ubiquitin ions characterized by electron capture dissociation. J. Am. Chem. Soc. **124**, 6407–6420 (2002)

58. Skinner, O.S., McLafferty, F.W., Breuker, K.: How ubiquitin unfolds after transfer into the gas phase. J. Am. Soc. Mass Spectrom. **23**, 1011–1014 (2012)

59. Hall, Z., Politis, A., Bush, M.F., Smith, L.J., Robinson, C.V.: Charge-state-dependent compaction and dissociation of protein complexes: insights from ion mobility and molecular dynamics. J. Am. Chem. Soc. **134**, 3429–3438 (2012)

60. Segev, E., Wyttenbach, T., Bowers, M.T., Gerber, R.B.: Conformational evolution of ubiquitin ions in electrospray mass spectrometry: molecular dynamics simulations at gradually increasing temperatures. Phys. Chem. Chem. Phys. **10**, 3077–3082 (2008)

61. Price, W.D., Schnier, P.D., Williams, E.R.: Tandem mass spectrometry of large biomolecule ions by blackbody infrared radiative dissociation. Anal. Chem. **68**, 859–866 (1996)

62. Guo, Y., Ling, Y., Thomson, B.A., Siu, K.W.: Combined ion-mobility and mass-spectrometry investigations of metallothionein complexes using a tandem mass spectrometer with a segmented second quadrupole. J. Am. Soc. Mass Spectrom. **16**, 1787–1794 (2005)